Journal of Sound and Vibration (2002) **256**(2), 197–211
doi:10.1006/jsvi.2001.3812, available online at http://www.idealibrary.com on IDEAL®

STUDY OF THE IMPINGEMENT OF IMPULSE WAVE UPON A FLAT PLATE

T. SETOGUCHI

Department of Mechanical Engineering, Saga University, Honjo-machi, Saga-shi, Saga 840-8502, *Japan*

H.-D. KIM

School of Mechanical Engineering, Andong National University, 388 *Songchun-dong, Andong* 760-749, *Korea. E-mail: kimhd@andong.ac.kr*

AND

H. KASHIMURA

Department of Control and Information Systems Engineering, Kitakyushu College of Technology Kokuraminami, Kitakyushu, Fukuoka 803-0985, *Japan*

(*Received* 20 *November* 2000, *and in final form* 2 *April* 2001)

The impulse wave is made by the weak normal shock discharge from an open end of a shock tube. In order to understand the dynamic characteristics of the impulse wave impinging upon a flat plate, experiments are performed over the shock Mach number range from 1·01 to 1·20. A flat plate is placed downstream, normal to the axis of the shock tube, to simulate the impulse wave impingement on an object. The distance between the exit of the shock tube and flat plate is changed. The baffle plate is installed at the exit of the shock tube. The sizes of the baffle plate and impinging flat plate are varied to investigate the magnitude of the impulse wave impinging upon the flat plate. Computational analysis is applied to model the flow field subject to unsteady, axisymmetric, inviscid, compressible, equations. Computational results well predict the experimented dynamic behavior of the impinging impulse wave. The impulse wave impinging upon the flat plate has a sharp peak of very short rising time and its magnitude decreases with distance from the center of the flat plate. The magnitude of the impulse wave impinging upon the flat plate can be predicted by the empirical equations that are developed in the present study.

1. INTRODUCTION

The pulse jet is usually generated by the sudden discharge of mass flow from the exit of a tube, and may be defined as a device capable of injecting a discrete pulse of fluid from a high-pressure chamber into a medium fluid or onto an object [1]. When the discharging mass flux is sufficiently large, the pulse jet leads to an impulsive wave propagating into the surroundings. Similar flows are made by the discharge of a shock wave from a tube exit, leading to a spherical blast wave that is usually characterized by a high peak pressure of short duration.

A major difference between pulse and continuous jets is the actual time behavior of the flow properties and the much higher-pressure ratio of the pulsed fluid to the surrounding medium fluid. For a continuous jet with a sufficiently high supply pressure, the flow structure is well understood. The jet spreading, the barrel shock structure, and the location

0022-460X/02/$35.00

of Mach disk have long been a major interest of the continuous supersonic jets [2, 3], and the flow field has been well established as functions of the jet pressure ratio, the detailed geometry of the tube, and the ratio of specific heats of the working gas employed. The gas pressure just upstream of the Mach disk and inside the barrel shock wave is, in general, very low compared to the back pressure, consequently leading to the strong entrainment of the surrounding gas into the jet flow.

The situation with the pulse jets is quite different. In this case the gas pressure just behind the spherical impulse wave is very high, compared to the back pressure level. The time-dependent wave behavior is the key factor characterizing the entire flow field. Therefore to understand the pulse jet flows, the dynamic characteristics of the impulse wave are more important than, for example, the turbulent mixing or entrainment.

Such impulse waves are encountered in a variety of unsteady internal flow devices, such as gun muzzles [4], internal combustion engine exhaust mufflers [5], high-speed railway tunnels [6], etc. In these applications, the impulse waves often cause annoying noises as well as pressure transients, which give rise to undesirable unsteady loads and structural vibrations. It is required that the impulse wave should be minimized by an appropriate control means [7, 8]. Much effort has been put on control of the magnitude of the impulse wave [7, 8], and the impulse wave has been reduced by as much as 50 per cent, depending on the shock Mach number yielded.

Meanwhile, there have been a number of practical applications in which a stronger impulse wave casts a better performance of the flow devices, such as pulse combustors [9], pulse jet filters [10], pulse jet cleanings [11], etc. The pulse jet devices for such purposes are now in commercial production or have recently been used for a variety of industrial fields. For example, in the semiconductor industry or coal-based power plants, removal of fine particles from surfaces is of practical importance both for surface cleaning and for contamination detection [12].

In spite of the fact that the relationship between the characteristics of the impulse wave and system performance has not been well understood, the impulse wave has been known to play an essential role in particle removal due to the start-up transients as the pulse jet is initiated. The current understanding of the flow fields that are produced by the impulse wave impingement upon an object is not enough for the purpose of design of practical applications. In such applications, it is of practical importance to predict the pressure transients and unsteady loads on an object. To the authors' knowledge, no effort to date has been put on this field.

The present paper describes experimental and computational work to understand the unsteady flows formed by the impulse wave impingement upon a flat plate. The impulse wave is made by a weak shock wave discharge from the open end of shock tube. An experiment is performed using a simple shock tube with an open end and computations are carried out to predict the corresponding unsteady, axisymmetric, inviscid, compressible, flow fields. The governing equations are solved numerically using the Harten–Yee TVD scheme [13]. The second order symmetric total variation diminishing (TVD) is incorporated into an operator splitting technique. In the present study, the distance between the exit of shock tube and plate, and the plate size are changed. A baffle plate is installed at the exit of the shock tube and its size is also changed to investigate the change in the unsteady flows produced on the impinging plate.

2. EXPERIMENTAL FACILITIES AND MEASUREMENT

The simple open-ended shock tube has a diameter (D) of 66 mm and a total length of about 3·77 m (the length of the driven section: 2·15 m), as shown in Figure 1. A sheet of

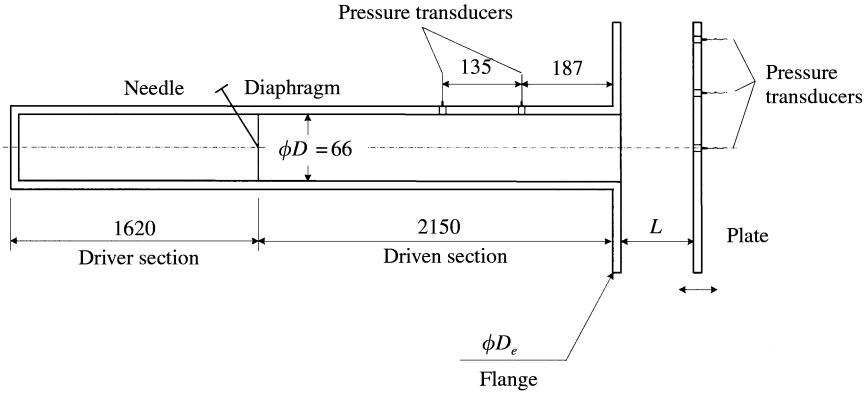

Figure 1. Experimental facility for the impulse wave impinging upon a flat plate.

cellophane 0·03 mm thick is used as a diaphragm, which is manually ruptured to initiate the wave motion. The initial pressure ratio of the shock tube is set to obtain shock Mach number, M, below 1·20, the driven air being initially at atmospheric pressure and room temperature.

In order to investigate the effects of the plate size on the major characteristics of the impinging impulse wave, the diameter of the flat plate D_p is varied in the range from 0·1D to 20 D (assumed that it is infinite). The distance (L) between the exit of the shock tube and flat plate is also changed in the range between 0·5 D and 4·0 D. This is to investigate the change in the impinging impulse wave with distance. According to the previous work [14, 15], the impulse wave which is formed by the weak shock discharge from an open end of a shock tube is strongly dependent on the detailed configurations of the tube exit. The effects of the baffle plate installed at the exit of the tube are extensively discussed [14, 15]. In the present study, the baffle plate having the diameter of D_e is installed at the exit of the shock tube. Its diameter is varied in the range from 1·0 D (no baffle plate) to 20 D (assumed that it is infinite) to investigate the effect of the baffle plate size on the impulse wave that is formed on the flat plate.

The initial pressures of the shock tube are monitored by a personal computer system. Calibrated pressure transducers, flush mounted on the shock tube walls at several stations are used to measure and characterize the shock wave propagating through the tube. In particular, static pressures at the positions of 322 mm (the measuring point ①) and 187 mm (the measuring point ②) from the exit of the shock tube are employed to establish the shock Mach number M. Other pressure transducers are flush mounted on the flat plate, to monitor the impinging impulse wave on it. The signals of the pressure transducer at the measuring point ② play a role of a trigger for visualizing the impulse wave discharged from the shock tube.

A schlieren system is incorporated into a delay circuit so that it allows the visualization of the impulse wave structure discharging from the shock tube at an instance. The light source for the schlieren system is provided by Mg strobrite spark lamp. The duration of the light flash is about 1 m. Output of the pressure transducer is recorded on an X–Y recorder by way of a wave memory. The pressure transducers were calibrated both statically and dynamically prior to each test. The uncertainty in pressure measurements is estimated to be less than $\pm$1·5 per cent. These estimations are based on the maximum possible fluctuations in the measurements.

3. COMPUTATIONAL ANALYSIS

The flow of the impulse wave impingement, discharged from the open end of the shock tube, upon the flat plate is simulated using a CFD method. Unsteady, axisymmetric, inviscid, conservation equations are solved numerically by assuming a perfect gas ($\gamma = 1{\cdot}4$),

$$\frac{\partial U}{\partial t} + \frac{\partial F}{\partial x} + \frac{\partial G}{\partial r} + H = 0, \tag{1}$$

$$U = \begin{bmatrix} \rho \\ \rho u \\ \rho v \\ e \end{bmatrix}, \quad F = \begin{bmatrix} \rho u \\ \rho u^2 + p \\ \rho uv \\ (e + p)u \end{bmatrix}, \quad G = \begin{bmatrix} \rho v \\ \rho uv \\ \rho v^2 + p \\ (e + p)v \end{bmatrix}, \quad H = \frac{1}{r}\begin{bmatrix} \rho v \\ \rho uv \\ \rho v^2 \\ (e + p)v \end{bmatrix},$$

where x is the longitudinal distance, r the radial distance, t the time, ρ the density and, u and v are the velocity components for x and r directions respectively. The total energy e per unit volume of the gas is expressed by the sum of the kinetic energy and the internal energy as follows:

$$e = \frac{p}{\gamma - 1} + \rho\left(\frac{u^2 + v^2}{2}\right). \tag{2}$$

Equation (1) is closed by the thermal equation of state of a perfect gas, $p = \rho RT$, where T is the temperature. In the computations, equation (1) is rewritten in non-dimensional form by referring the quantities, the pressure, density, etc., to atmospheric conditions and the diameter of the shock tube:

$$x' = \frac{x}{D}, \quad r' = \frac{r}{D}, \quad u' = \frac{u}{a_a/\sqrt{\gamma}}, \quad v' = \frac{v}{a_a/\sqrt{\gamma}},$$

$$t' = \frac{t}{\sqrt{\gamma}D/a_a}, \quad p' = \frac{p}{p_a}, \quad \rho' = \frac{\rho}{\rho_a}, \quad e' = \frac{e}{p_a}. \tag{3}$$

Superscript ($'$) indicating the non-dimensional quantities is omitted for the sake of simplicity. The subscript a denotes atmospheric state ahead of the shock wave. The resulting non-dimensional form of equation (1) is solved numerically using the Harten–Yee TVD scheme [13]. The second order symmetric total variation diminishing (TVD) is incorporated into the operator splitting technique which was suggested by Sod [15].

Figure 2 shows the computational domain and boundary conditions used in computation. For setting up the initial conditions, a normal shock with its overpressure Δp^* is assumed to be discharged from the tube exit. The inflow and outflow conditions are applied to the upstream and downstream boundaries respectively. The symmetric conditions at the centerline of the tube reduce the computational effort for a full domain, and the slip-wall conditions are applied to the solid walls. The upstream boundary is located well back within the shock tube so as to allow for an expansion wave to travel back upstream. The downstream boundaries are somewhat varied depending on the shock Mach number, but far enough to avoid the unwanted wave reflections from the boundaries. A square grid system is used to characterize the impulse waves discharged from the open end of the tube.

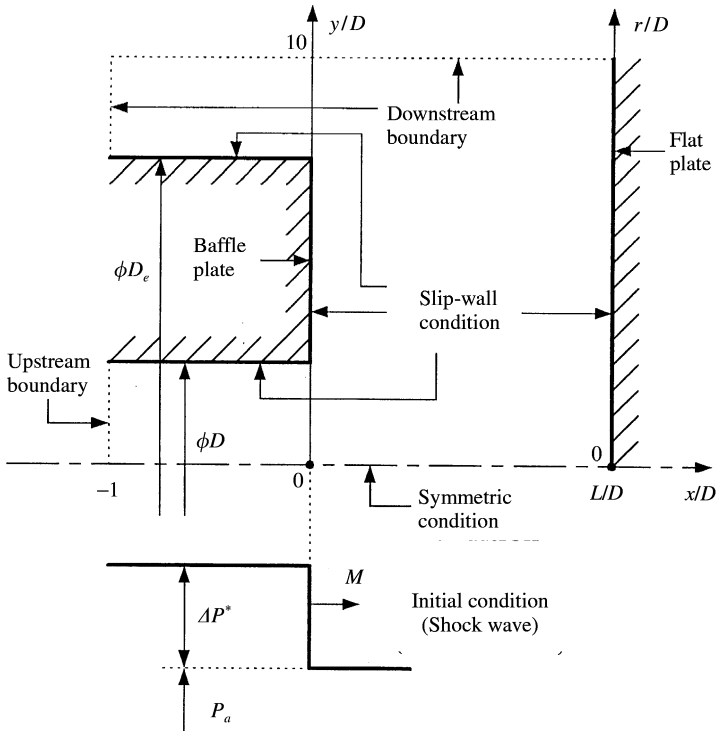

Figure 2. Flow field for computation and boundary conditions.

The fineness of computational grid required to obtain grid-independent solutions was first examined for some of the impulse waves discharged from the exit of the shock tube. The grid density over $\Delta x = \Delta y = 70/D$ seemed to change the accuracy of obtained solutions no longer. A grid size of $\Delta x = \Delta y = 75/D$ is employed in the present computations which ensure that the solutions obtained were independent of the grid density.

4. RESULTS AND DISCUSSION

Figures 3 and 4 present schlieren pictures and computed iso-density contours showing the impulse wave forms for $L/D = 0{\cdot}5$ and $1{\cdot}0$ respectively. D_e/D and D_p/D are kept constant by 20, and the shock Mach number M is $1{\cdot}07$. Both experimented and computed wave forms are obtained for the same t' which is the time elapsed from the instance the normal shock passes over the measuring point ②. In Figure 3(a), the impulse wave is for an instance ($t' = 0{\cdot}212603$) just after the normal shock wave inside the shock tube discharges from the open end of the shock tube. It is visible that the impulse wave is a cylindrical form, being nearly a plane wave close to the axis of the tube. At the corner of the tube exit, the wave refractions are observed from both experiment and computation. It seems that the present computation predicts the experimented wave forms well. In Figure 3(b) the wave form is taken for an instance ($t' = 0{\cdot}460638$) just after the impulse wave impinges on the flat plate. It is again found that the computed wave forms are in good agreement with the experimented ones. In Figure 4(b), the impulse wave just after the impingement on the flat plate is nearly spherical. It is found that the reflected wave from the flat plate propagates upstream toward

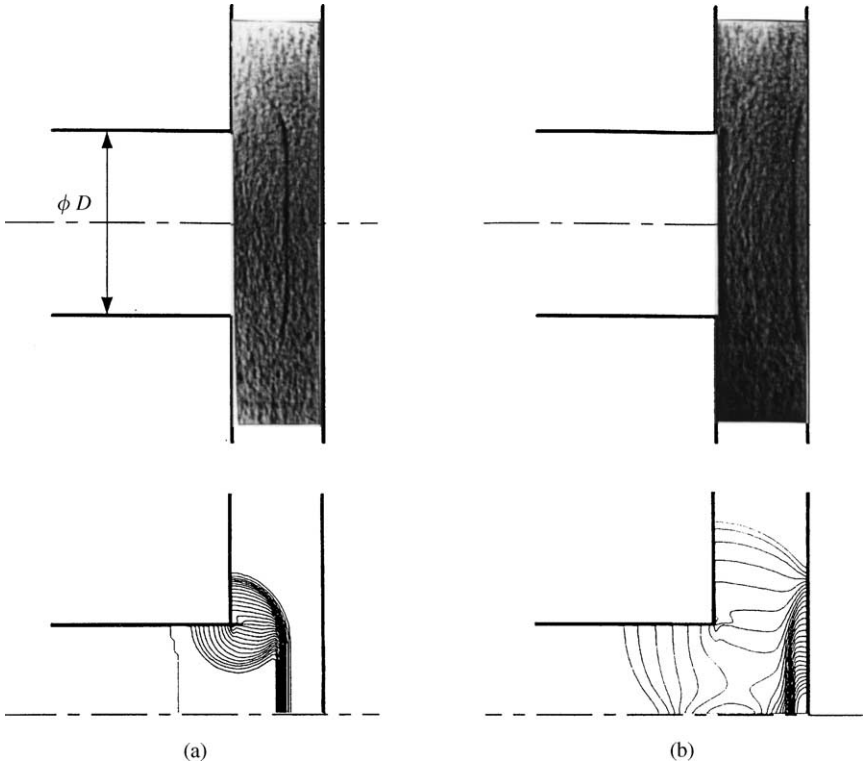

Figure 3. Schlieren pictures showing impulse wave and computed iso-density contours ($L/D = 0{\cdot}5$, $D_e/D = D_p/D = 20$, $M = 1{\cdot}07$): (a) $t' = 0{\cdot}212603$, $\Delta\rho = 0{\cdot}004736$ kg/m^3; (b) $t' = 0{\cdot}460638$, $\Delta\rho = 0{\cdot}009885$ kg/m^3.

the baffle plate. From the computational results it is observed that the expansion waves propagate back inside the shock tube.

Figure 5 shows a comparison of the time histories of the computed and measured static pressure generated on the flat plate, where D_e/D and D_p/D are the same being 20. The static pressure on the flat plate suddenly rises up to a peak value, strongly depending on the shock Mach number and location on the plate. After the peak value, the static pressure sharply decreases with time. It seems that the peak pressure value decreases nearly exponentially with the distance in radial direction. From this time history of the static pressures produced on the flat plate, it is known that the pulse wave has a sharp peak of a very short rising time. The rising time for the pressure to reach the peak value seems to be longer with the distance in radial direction. The present computations predict the peak value and rising time of the experimented pressures well.

For $M = 1{\cdot}10$, $L/D = 0{\cdot}5$ and $D_e/D = D_p/D = 20$, Figure 6 shows the computational results of iso-density contours and the static pressures in both the axial and radial directions. On the flat plate the static pressure has a peak value and sharply decreases with the radial distance. At the center of the flat plate, the peak pressure is about 1·54 times the atmospheric pressure (P_a). From the static pressure distribution in axial direction, the static pressure is constant at the region of $x/D < -0{\cdot}3$; this value corresponds to that of static pressure just downstream of a normal shock wave of $M = 1{\cdot}10$. The static pressure decreases with the axial distance in the region from $x/D = -0{\cdot}3$ to $0{\cdot}3$. This is due to the expansion waves generating at the exit plane of the shock tube. The static pressure suddenly rises as the flow meets the reflected impulse wave from the flat plate.

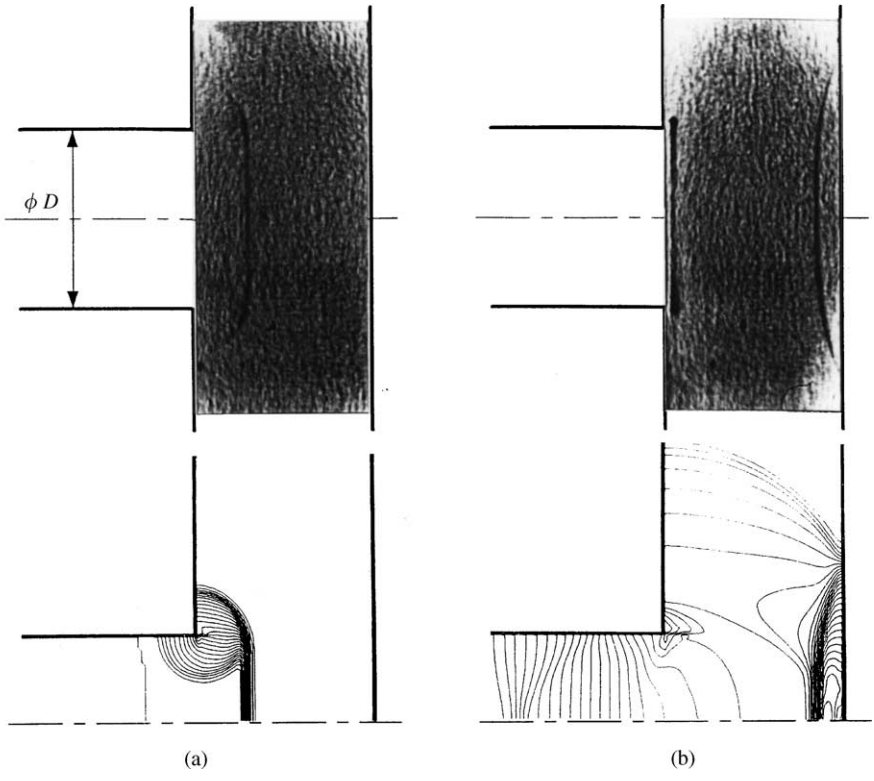

Figure 4. Schlieren pictures showing impulse wave and computed iso-density contours ($L/D = 1{\cdot}0$, $D_e/D = D_p/D = 20$, $M = 1{\cdot}07$): (a) $t' = 0{\cdot}212603$, $\Delta\rho = 0{\cdot}004736$ kg/m^3; (b) $t' = 0{\cdot}871673$, $\Delta\rho = 0{\cdot}005367$ kg/m^3.

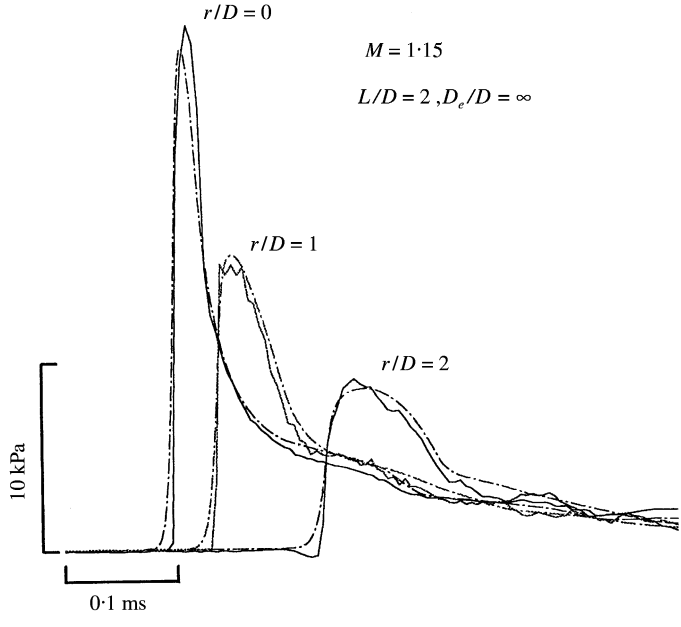

Figure 5. Time histories of the static pressure on the flat plate ($L/D = 2{\cdot}0$, $D_e/D = D_p/D = 20$, $M = 1{\cdot}15$): ——, experiment; – · – · –, calculation.

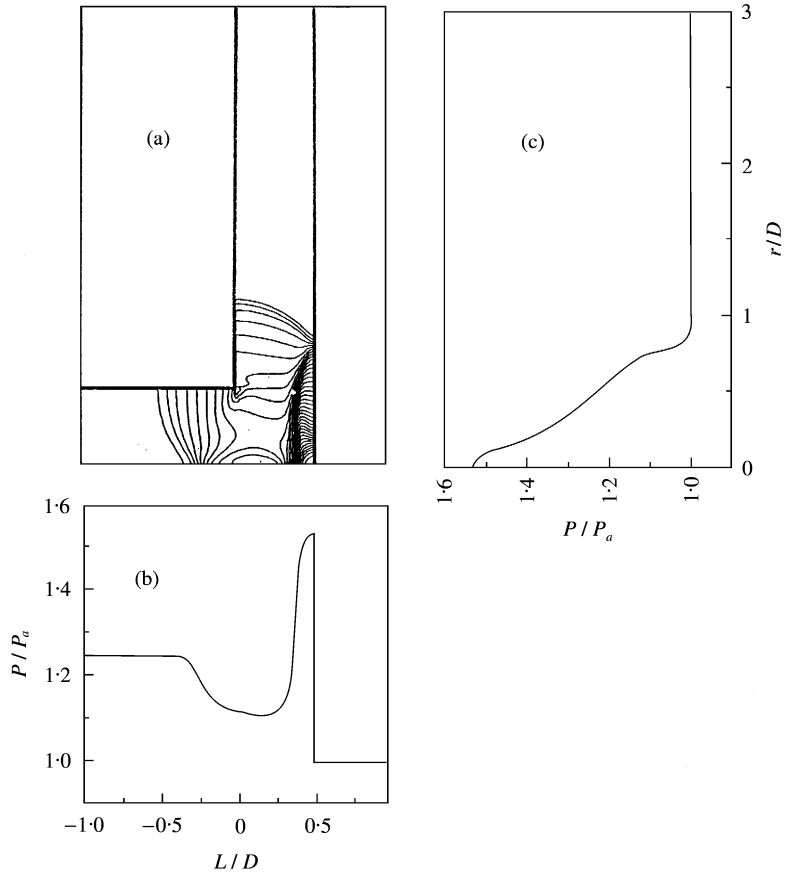

Figure 6. Computed iso-density contours, static pressure distributions on the flat plate and along the tube axis ($D_e/D = D_p/D = 20$, $L/D = 0{\cdot}5$, $M = 1{\cdot}1$ and $t' = 0{\cdot}47293$).

Figure 7 shows the static pressure variations along the tube axis and on the flat plate, where $L/D = 2{\cdot}0$, $D_e/D = 1{\cdot}0$, $D_p/D = 20$ and $M = 1{\cdot}10$. In the static pressure distribution in radial direction, the peak pressure occurs at $r/D = 1{\cdot}0$, and the pressure at the center of the flat plate is lower than that at $r/D = 1{\cdot}0$. From the static pressure distribution in axial direction it is found that the constant pressure which is nearly the same as atmospheric pressure exists in the region between $x/D = 0{\cdot}2$ and $1{\cdot}6$.

In practical industrial applications making use of pulse wave, it is of importance to predict the peak pressure that occurs at object surface. For $D_e/D = D_p/D = 20$, $L/D = 0{\cdot}5$, Figure 8 shows the peak pressure ΔP_m produced on the flat plate with the shock Mach number M. The peak pressure is normalized by the overpressures ΔP^* of each of the shock waves (see Figure 2). At the center of the flat plate, the normalized peak pressure increases with M, but at the locations of $r/D = 1{\cdot}0$ and $2{\cdot}0$, it nearly remains constant or slightly decreases with an increase in Mach number. In these cases, no appreciable change in the peak pressure is found with the Mach number. The present computations well predict this trend of experimental results.

Figure 9 shows the effect of L/D on the peak pressures on the flat plate, where $M = 1{\cdot}07$ and $D_e/D = D_p/D = 20$. At the center of the flat plate, the normalized peak pressure greatly decreases with L/D. But at the locations of $r/D = 1{\cdot}0$ and $2{\cdot}0$, it does not strongly depend on

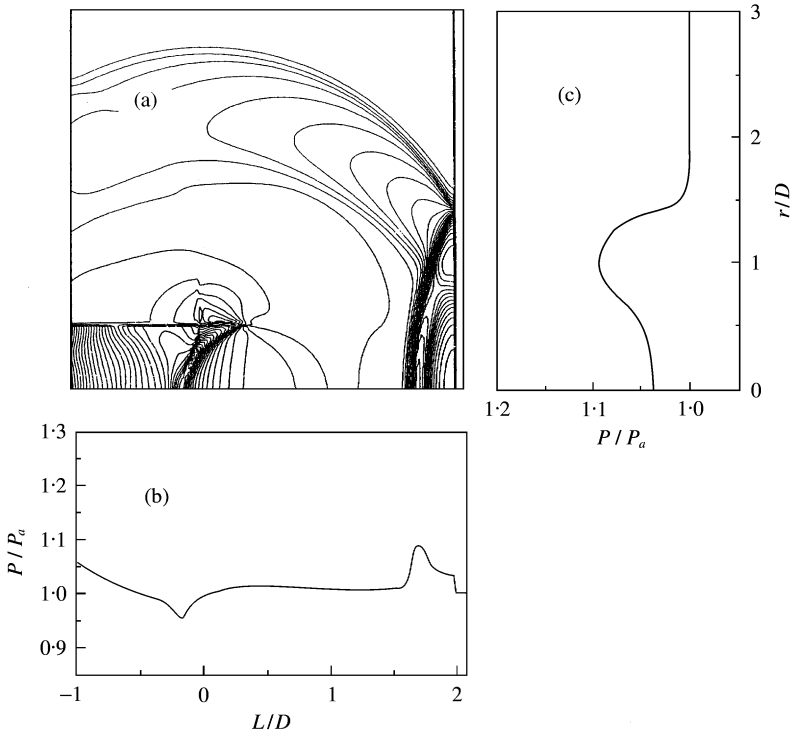

Figure 7. Computed iso-density contours, static pressure distributions on the flat plate and along the tube axis ($D_e/D = 1{\cdot}0$, $D_p/D = 20$, $L/D = 2{\cdot}0$, $M = 1{\cdot}1$ and $t' = 1{\cdot}75659$).

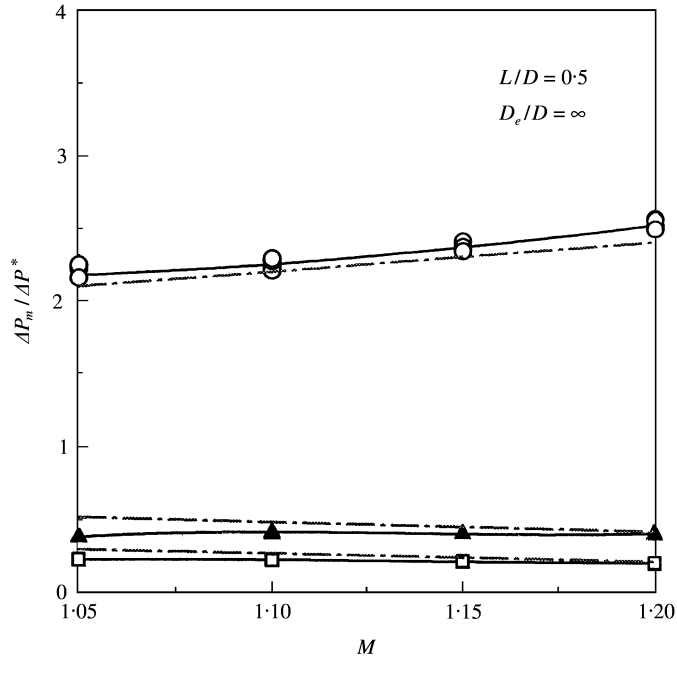

Figure 8. Variation of the peak pressure on the flat plate with M ($L/D = 0{\cdot}5$, $D_e/D = D_p/D = 20$): experiment r/D, —○—, 0; —▲—, 1; —□—, 2; – · – · –, calculation.

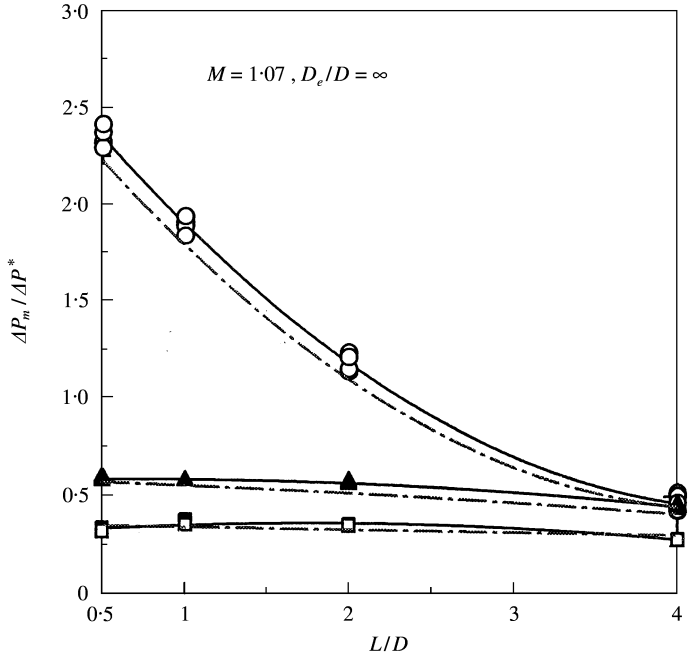

Figure 9. Variation of the peak pressure on the flat plate with L/D ($D_e/D = D_p/D = 20$, $M = 1{\cdot}07$): –·–·–, calculation; experiment r/D, —○—, 0; —▲—, 1; —□—, 2.

the value of L/D. For $L/D = 0{\cdot}5$, the peak pressure produced at the center of the flat plate is nearly 2·4 times the overpressure of the normal shock wave of $M = 1{\cdot}07$. The present data of both measured and computed peak pressures show that the peak pressure at the center of the flat plate can be a function of M and L/D.

For a small flat plate, it is expected that the peak pressure would be influenced by the expansion wave systems from the edges of the flat plate as well as impulse wave reflections on the flat plate. In order to investigate the effect of the flat plate size on the peak pressure at the center of the flat plate, the diameter of the flat plate is changed in the range from $D_p/D = 0{\cdot}1$ to 20. Figure 10 shows the computed time histories of the static pressures on the flat plate, where $M = 1{\cdot}05$, $D_e/D = 20$, and $L/D = 1{\cdot}0$. There are two major changes in the wave forms with D_p/D; one is the peak pressure at the center of the flat plate, and the other is the pressures after the reflection of the impulse wave from the flat plate. It is interesting to find that for small D_p/D values the peak pressure increases with an increase in D_p/D, but it does no longer change for the flat plates of $D_p/D > 0{\cdot}5$. The static pressures after the impulse wave reflection are strongly dependent on D_p/D, associated with the expansion wave systems generated from the edges of the flat plate. Figure 11 shows the relationship between the peak pressure at the center of the flat plate and D_p/D. The peak pressure is essentially constant for the flat plates larger than $D_p/D = 0{\cdot}5$. With regard to the peak pressure occurring at the center of the flat plate, it is thus believed that a flat plate larger than $D_p/D = 0{\cdot}5$ would be of an infinite flat plate.

Figure 12(a) and 12(b) present the effect of the baffle plate size D_e/D on the static pressure at the center of the flat plate for $L/D = 0{\cdot}5$ and 2·0 respectively. With D_e/D, there are some changes in the pressures, after the impulse wave reflections from the flat plate. However, it does not seem that the peak pressure changes with D_e/D. It is, therefore, concluded that the

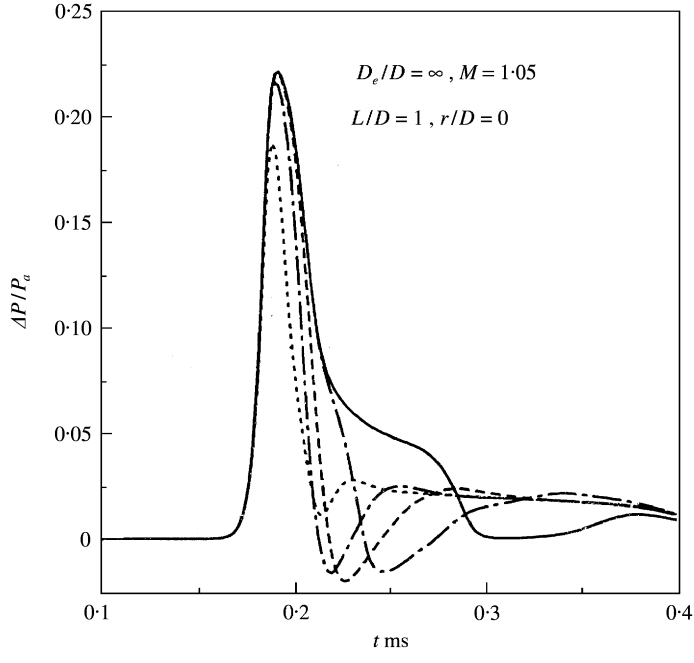

Figure 10. Computed time histories of the static pressure at the center of the flat plate ($D_e/D = 20$, $L/D = 1{\cdot}0$, $M = 1{\cdot}05$ and $r/D = 0{\cdot}0$). D_p/D: ——, 1; – · – · –, 0·5; – – –, 0·3; — · — · —, 0·2; - - - - -, 0·1.

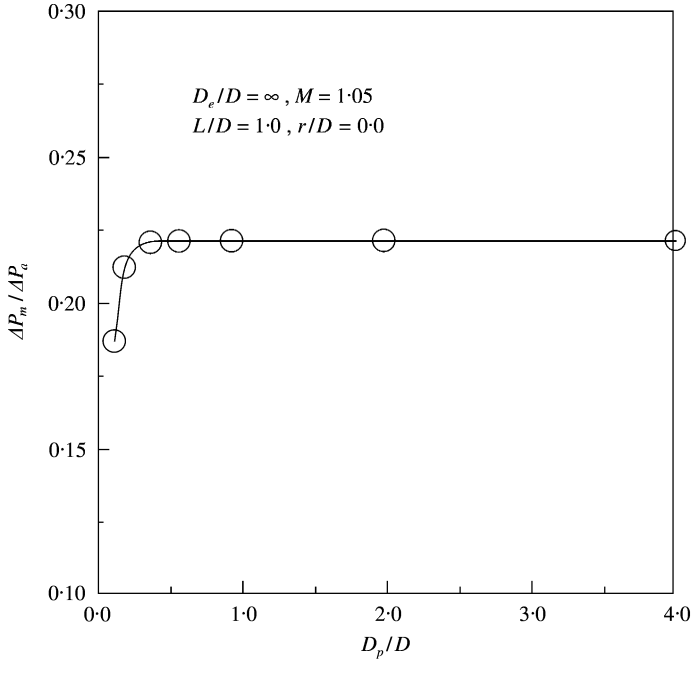

Figure 11. Relationship between the peak pressure at the center of the flat plate and D_p/D.

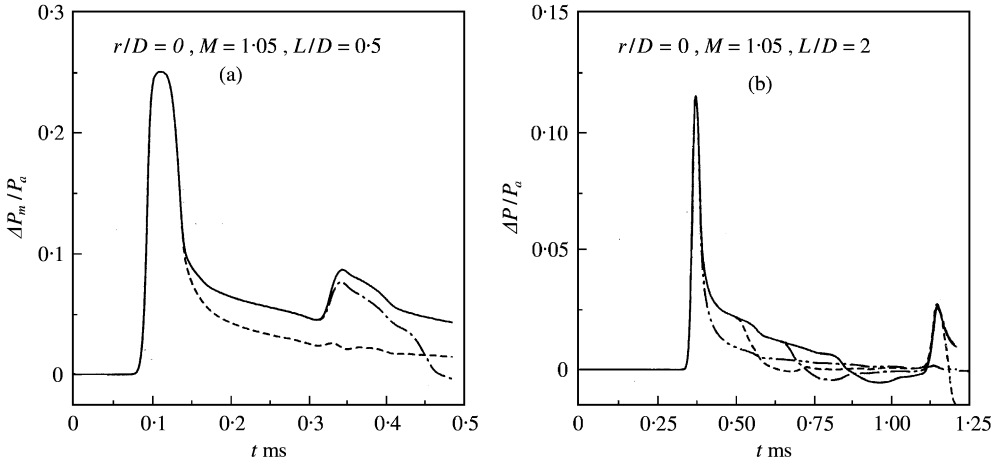

Figure 12. Computed time histories of the static pressure at the center of the flat plate ($D_p/D = 20$, $M = 1{\cdot}05$, and $r/D = 0{\cdot}0$) (a) $L/D = 0{\cdot}5$. D_e/D: ——, 3, 4, ∞; – · – · –, 2; - - - - -, 1. (b) $L/D = 2{\cdot}0$. D_e/D: ——, 4, ∞; – · – · –, 3; - - - - -, 2; – · · – · · –, 1.

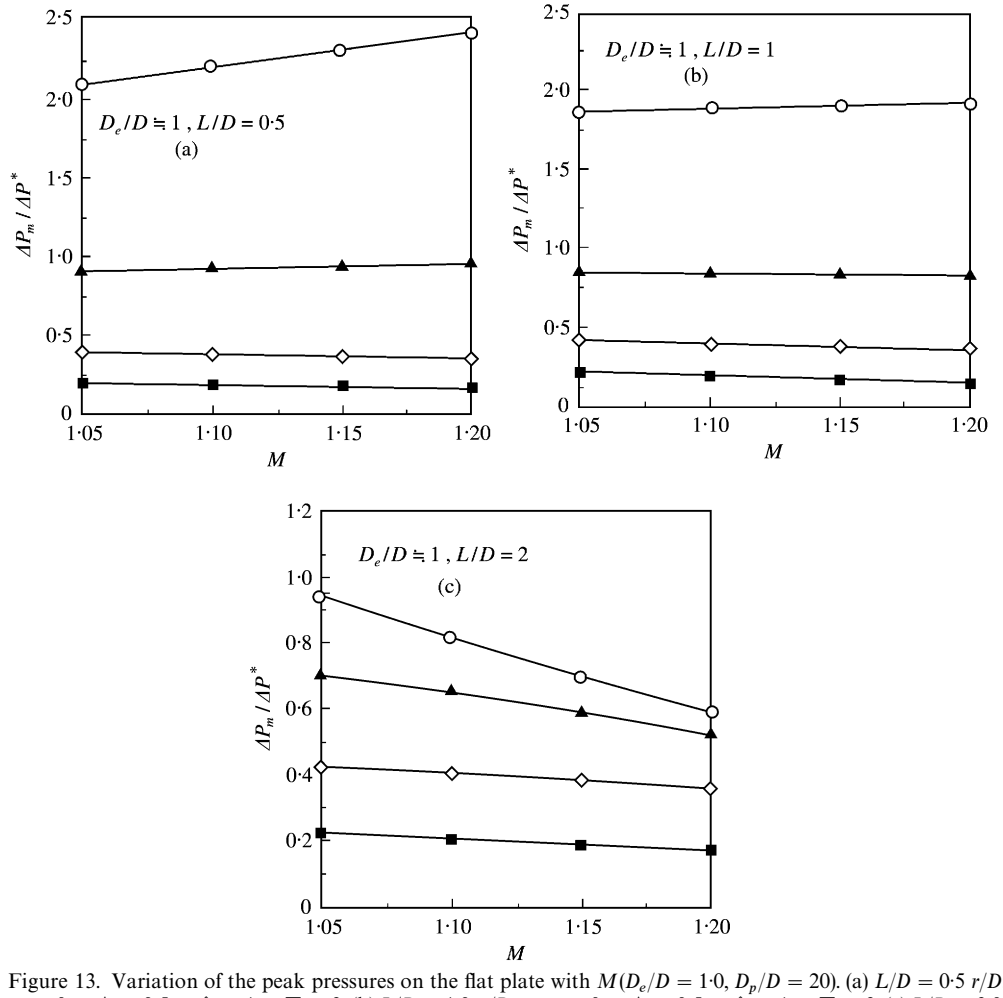

Figure 13. Variation of the peak pressures on the flat plate with M ($D_e/D = 1{\cdot}0$, $D_p/D = 20$). (a) $L/D = 0{\cdot}5$ r/D: —○—, 0; —▲—, 0·5; —◇—, 1; —■—, 2. (b) $L/D = 1{\cdot}0$. r/D: —○—, 0; —▲—, 0·5; —◇—, 1; —■—, 2. (c) $L/D = 2{\cdot}0$. r/D: —○—, 0; —▲—, 0·5; —◇—, 1; —■—, 2.

presence of the baffle plate at the exit of tube does not affect the peak pressure at the center of the flat plate.

Figure 13 represents the relationship between the normalized peak pressures ΔP_m on the flat plate and shock Mach number M. Note that D_e/D is kept constant by 1·0 (no baffle plate). For $L/D = 0{\cdot}5$ of Figure 13(a), the normalized peak pressure at $r/D = 0{\cdot}0$ increases with M. But at $r/D = 0{\cdot}5$ it is nearly constant with M. At the locations of $r/D > 0{\cdot}5$, it seems to decrease only slightly with M. For $L/D = 1{\cdot}0$, the normalized peak pressure rises slightly with M, but at the locations of $r/D > 0{\cdot}5$, it decreases slightly with M. For $L/D = 2{\cdot}0$ of Figure 13(c), the normalized peak pressures decrease with M at all the locations on the flat plate. It seems that the decreasing rate in the peak pressure with M is highest at the center of the flat plate.

The above data all showed that for $D_p/D > 0{\cdot}5$ the peak pressure produced on the flat plate does not depend on the baffle plate but on L/D and M. The present data are collected to obtain some empirical prediction for the peak pressure on the flat plate. Figure 14(a) presents the correlation of the peak pressures at the center of the flat plate. It is found that all data show a good correlation for a given value of M and L/D. A best fit is given by

$$\left(\frac{\Delta P_m}{P_a}\right)_{r/D=0} = 0{\cdot}10\, M^{10{\cdot}322} \cdot \left(\frac{L}{D}\right)^{-1{\cdot}110}, \tag{4}$$

where $(\Delta P_m/P_a)_{r/D=0}$ means the peak pressure at the center of the flat plate, normalized by the atmospheric pressure P_a. From equation (4) the peak pressure ΔP_m can be predicted with a good accuracy. Using the known peak pressure at the center of the flat plate, the peak pressure at a location in radial direction on the flat plate can be predicted by

$$\left(\frac{\Delta P_m}{P_a}\right)_{r/D} = 0{\cdot}31 \left(\frac{\Delta P_m}{P_a}\right)_{r/D=0} \cdot \left(\frac{r}{D}\right)^{-0{\cdot}85}, \tag{5}$$

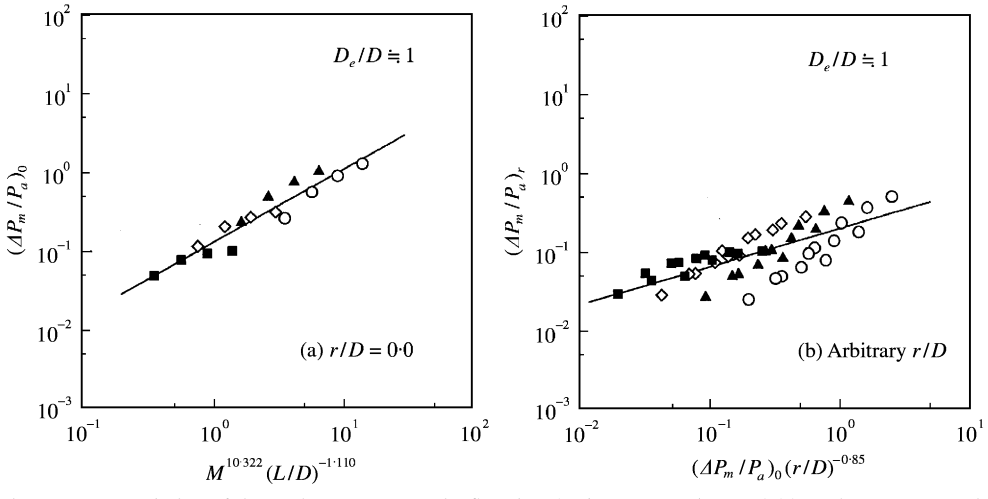

Figure 14. Correlation of the peak pressures on the flat plate ($D_e/D = 1{\cdot}0$, $D_p/D = 20$) (a) Peak pressures at the center of the flat plate. L/D: ○, 0·5; ▲, 1; ◇, 2; ■, 4. (b) Peak pressures at an arbitrary location in radial direction on the flat plate. L/D: ○, 0·5; ▲, 1; ◇, 2; ■, 4.

where $(\Delta P_m/P_a)_{r/D}$ means the peak pressure at an arbitrary location on the flat plate. Figure 14(b) shows that equation (5) provides a good prediction for the peak pressures at an arbitrary location on the flat plate.

5. CONCLUSIONS

The present paper describes experimental and computational work to investigate the dynamic characteristics of the impulse wave impingement upon a flat plate. The impulse wave is made by the weak normal shock discharge from an open end of a shock tube. Experiments are performed using an open-ended shock tube over the shock Mach number range from 1·01 to 1·20. A flat plate is placed downstream, normal to the axis of the shock tube, to simulate the impulse wave impingement on an object. The distance between the exit of the shock tube and flat plate is changed. The baffle plate is installed at the exit of the shock tube. The sizes of the baffle plate and impinging flat plate are varied to investigate the magnitude of the impulse wave impinging upon the flat plate. Computational analysis is applied to model the flow field subject to unsteady, axisymmetric, inviscid, compressible, equations. A TVD numerical scheme is used to solve the conservation equation systems. Computational results well predict the dynamic behavior of the impinging impulse wave. The impulse wave impinging upon the flat plate has a sharp peak of very short rising time and its magnitude decreases with distance from the center of the flat plate. The magnitude of the impulse wave impinging upon the flat plate can be predicted by the empirical equations that are developed in the present study. For the flat plates larger than 0·5 times the diameter of the tube the magnitude of the impulse wave at the center of the flat plate is not dependent on the flat plate size. The baffle plate installed at the exit of the tube does not affect the magnitude of the impulse wave at the center of the flat plate.

REFERENCES

1. S. RAGHUNATHAN, H. D. KIM and T. SETOGUCHI 1998 *Progress in Aerospace Sciences* **34**, 1–44. Impulse noise and its control.
2. T. C. JR. ADAMSON and A. NICHOLLS 1959 *Journal Aerospace Sciences* **26**, 16–24. On the structure of jets from highly underexpanded nozzles into still air.
3. F. S. SHERMAN 1966 *Rarefied Gas Dynamics* **2**, 84–105. The structure and utilization of supersonic free jets in low density wind tunnels.
4. G. KLINGENBERG and J. M. HEIMERL 1992 *Gun Muzzle Blast and Flash. Progress in Astronautics and Aeronautics, AIAA Educational Series.*
5. N. SEKINE, S. MATSUMURA, K. AOKI and K. TAKAYAMA 1989 17*th International Symposium on Shock Wave and Shock Tubes*, 671–676. Generation and propagation of shock waves in the exhaust pipe of a four cycle automobile engine.
6. K. MASTUO and T. AOKI 1992 18*th International Symposium on Shock Wave and Shock Tubes.* Wave problems in high-speed railway tunnel.
7. T. SETOGUCHI, H. D. KIM, S. YU and S. RAGHUNATHAN 1999 *Journal of Thermal Sciences* **8**, 1–8. Passive control of an impulsive wave using a cavity/helical vane system.
8. H. D. KIM, T. SETOGUCHI, H. KASHIMURA and S. RAGHUNATHAN 2000 *IMECH, Journal of Mechanical Engineering Science* (to be published). Augmentation of the magnitude of the impulsive wave discharging from an open end of a duct.
9. J. A. C. KENTFIELD 1993 *Nonsteady, One-Dimensional, Internal, Compressible Flows* (*Theory and Applications*). Oxford: Oxford University Press, Chapter 7.
10. R. KLINGEL and F. LOFFLER 1983 *Proceedings of the Filtration Society, Filtration and Separation* **20**, 205–208. Dust collection and cleaning efficiency of a pulse jet fabric filters.
11. W. J. MORRIS 1984 *Proceedings of the Filtration Society, Filtration and Separation* **21**, 52–54. Cleaning Mechanisms in pulse jet fabric filters.

12. G. T. SMEDLY, D. T. PHARES and R. C. FLAGAN 1998 *Experiments in Fluids* **26**, 116–125. Entrainment of fine particles from surfaces by impinging shock waves.
13. H. C. YEE 1987 *NASA TM*-89464. Upwind and symmetric shock capturing schemes.
14. H. D. KIM and T. SETOGUCHI 2000 *American Institute of Aeronautics and Astronautics* (to be published) Weak shock reflection from an open end of a tube with baffle plate.
15. H. D. KIM and T. SETOGUCHI 1999 *Journal of Sound and Vibration* **226**, 1011–1028. Study of the discharge of weak shocks from an open end of a duct.
16. G. A. SOD 1977 *Journal of Fluid Mechanics* **83**, 785–794. A numerical study of a converging cylindrical shock.

APPENDIX A: NOMENCLATURE

a	speed of sound
D	diameter
e	total energy per unit volume
M	shock wave Mach number
L	distance between tube exit and flat plate
p	static pressure
r	radial distance
t	time
u	velocity component in x direction
v	velocity component in y direction
x	longitudinal distance in cylindrical co-ordinate
y	radial distance in cylindrical co-ordinate
γ	ratio of specific heats
ρ	density

Super/subscripts

a	atmospheric state
e	baffle plate
p	flat plate
m	peak or maximum value
$*$	normal shock wave overpressure
$'$	non-dimensional quantity